analytical chemistry

ARTICLE

pubs.acs.org/ac

Highly Sensitive Fluorescent Analysis of Dynamic Glycan Expression on Living Cells Using Glyconanoparticles and Functionalized Quantum Dots

En Han, Lin Ding, and Huangxian Ju*

State Key Laboratory of Analytical Chemistry for Life Science, Department of Chemistry, Nanjing State University, Nanjing 210093, China

ABSTRACT: A double signal amplification strategy was designed for highly sensitive and selective in situ monitoring of carbohydrate on living cells. The double signal amplification included the multiplex sandwich binding of functionalized quantum dots (QDs) to both glycan groups on the cell surface and glyconanoparticles and a cadmium cation sensitized fluorescence emission of Rhod-5N. Using the sialic acid−phenylboronic acid recognition system as a model, the 3-aminophenylboronic acid functionalized QDs (APBA−QDs) were synthesized by covalently binding APBA to mercaptopropionic acid capped CdS QDs, and the glyconanoparticles, polysialic acid stabilized gold nanoparticles (PSA−AuNPs), were prepared by a one-pot procedure. The APBA−QDs first recognized the sialic acid (SA) groups on BGC-823 human gastric carcinoma (BGC) cells and then the PSA on AuNPs, which were further used to bind more APBA−QDs on the cell surface for signal amplification. After the bound QDs were dissolved to release the Cd^{2+}, a Cd^{2+}-sensitized fluorescence method was developed for the detection of BGC cells in a linear range from 5.0×10^2 to 1.0×10^7 cells mL^{-1} with a limit of detection down to 210 cells mL^{-1} (8 cells in 40 μL of solution) and the dynamic monitoring of SA expression variation on the cell surface. The monitoring result was identical with that from flow cytometric analysis. This approach showed high specificity and acceptable reproducibility. This strategy provided a promising platform for highly sensitive cytosensing and cytobiologic study.

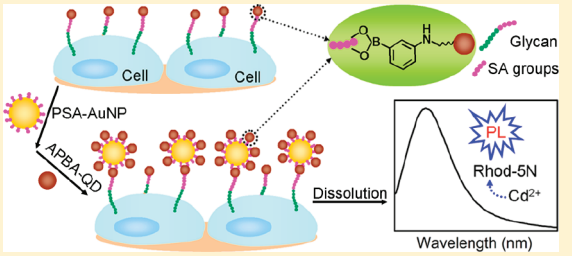

Glycosylation has been recognized as one of the most common post-transcriptional modifications of proteins in eukaryotes.[1−3] As the glycosylation products, glycoproteins on the cell surface play key roles in a wide variety of biological processes, including cellular adhesion, cell signaling, cell−cell communication, and immune response.[4−7] The changes in cell surface glycoproteins have been demonstrated to be associated with many diseases, such as inflammation and cancers.[8−10] For example, the overproduction of sialic acid (SA) groups has been found on colorectal cancer cells as compared to normal control.[11] Moreover, tumor-associated alterations of cell surface glycans play crucial roles in metastasis of carcinoma cells by altering tumor cell adhesion or motility.[12,13] Therefore, sensitive analysis of glycoproteins or glycans on living cells is keenly desirable for basic science advancement, clinical diagnostics, and therapeutics.[14]

Some methods including mass spectrometry and chromatography are powerful for glycomic detection, but these techniques are unsuitable for detection of living cell interrogation due to their destructivity.[15,16] The use of lectins and antibodies with defined glycan specificities[17] offers alternative nondestructive tools to profile cell surface glycan expression at different developmental stages of disease.[18] These tools, including lectin-array-based microscopic approaches[19−21] and probe-tagged lectin-based electrochemical strategies,[22−25] have shown great promise. However, they generally suffer from the poor specificity of lectins.[26] Meanwhile, the utilization of lectin- or antibody-based technology might be hindered by either high cost or relatively poor stability of proteins themselves.[27] Thus, developing new methods with high sensitivity and specificity is of significant advantage in the study of glycobiology.

Phenylboronic acid (PBA), a synthetic molecule, has been demonstrated to make stable complexes with sugars containing 1,2- or 1,3-diol structures such as mannose and galactose at the pHs higher than its pK_a value of 8.63.[28−30] However, recent works have suggested that SA can exceptionally form stable binding with undissociated PBA at physiological pH of 7.4.[31−33] The anomalous complexing ability is correlated to the different binding modality of the PBA−SA complex from other sugars.[31] This interesting finding provides an innovating molecular targeting platform for monitoring the expression of SA groups on living cells. Thus, PBA-functionalized quantum dots (QDs) have recently been prepared for detection of SA on a cell surface by cell imaging.[34] This work made use of the specific recognition of PBA to SA to develop a sandwich recognition of 3-aminophenylboronic acid (APBA)-functionalized QDs to cell surface SA groups and polysialic acid-stabilized AuNPs (PSA−AuNPs). By the enrichment of APBA−QDs on the bound PSA−AuNPs on the cell surface, a newly designed signal amplification method was thus developed for highly sensitive monitoring of SA on living cells.

Received: March 30, 2011
Accepted: August 2, 2011
Published: August 02, 2011

Nanomaterials such as AuNPs, carbon nanotubes, magnetic nanobeads, and QDs have extensively been used to enhance the signal intensity of recognition event for improving the detection sensitivity of a target.[35−38] By dissolving the Cd^{2+}-based QDs as a label probe, the recognition event and the target can conveniently be detected by anodic stripping voltammetric analysis of cadmic cation.[37,38] This technique has become a popular electrochemical method for the detection of protein,[37] DNA,[39] and cells.[22] Recently, the sensitizing effect of cadmium cation on the fluorescence signal of nonfluorescent metal-sensitive dyes such as Fluo-4 and Rhod-5N has been reported.[40] The triggered fluorescence results from the structure change of the metal-responsive fluorophore due to the binding of cadmium cation, which greatly increases the quantum yield and makes the non- or weakly fluorescent dye molecules become highly fluorescent. This property can produce hundreds-fold enhancement in signal intensity and has been used for sensitive detection in bioassays.[40,41] By combining the sensitizing effect of cadmium cation on fluorescence emission of Rhod-5N with the enrichment of APBA−QDs on one recognition event of APBA to the cell surface SA groups, here a double signal amplification strategy was designed for highly sensitive fluorescent analysis of cells down to eight human gastric carcinoma (BGC) cells with a wide linear range and dynamic fluorescent monitoring of SA expression variation on the cell surface. The proposed method possessed potential applications in clinical diagnosis and elucidation of carbohydrate functions on living cell surface.

EXPERIMENTAL SECTION

Reagents. $AuCl_3HCl\cdot 4H_2O$ (>48% Au) and sodium citrate were obtained from Shanghai Chemical Reagent Co., Ltd. (China). Rhod-5N was purchased from Invitrogen (U.S.A.). Cadmium chloride ($CdCl_2\cdot 2.5H_2O$) was purchased from Alfa Aesar China Ltd. Mannose, galactose, thioacetamide, and sodium borohydride were purchased from Sinopharm Chemical Reagent Co., Ltd. (China). Sialidase, 3-aminophenylboronic acid monohydrate (APBA), bovine serum albumin (BSA), polysialic acid (PSA), 1-ethyl-3-(3-dimethylaminopropyl) carbodiimide (EDC), mercaptopropionic acid (MPA), SA, and fluorescein isothiocyanate (FITC) were purchased from Sigma-Aldrich Inc. (U.S.A.). All other reagents were of analytical grade. Phosphate-buffered saline (PBS, 0.01 M, pH 7.4) contained 136.7 mM NaCl, 2.7 mM KCl, 8.7 mM Na_2HPO_4, and 1.4 mM KH_2PO_4. All aqueous solutions were prepared using ultrapure water (≥18 MΩ, Milli-Q, Millipore).

Apparatus. The UV−vis absorption and photoluminescence spectra were recorded with a UV-3600 UV−vis−near-infrared (NIR) spectrophotometer (Shimadzu, Japan) and a F900 fluorescence spectrometer (Edinburgh Instruments Ltd., U.K.), respectively. The transmission electron microscopic (TEM) image was observed on a JEM-2100 transmission electron microscope (JEOL Ltd., Japan). X-ray photoelectron spectroscopic (XPS) measurements were performed with an ESCALAB 250 spectrometer (Thermo-VG Scientific, U.S.A.) with an ultrahigh vacuum generator. Infrared spectra were recorded on a Nicolet 400 Fourier transform infrared (FT-IR) spectrometer (Madison, WI). The dynamic light scattering experiment was carried out using a Brookhaven BI-9000AT instrument (Brookhaven Instruments Corporation). Confocal images of cells were obtained using a confocal microscope (TCS SP5 Leica, Germany) with the laser excitation wavelength of 476 nm at room temperature.

Scheme 1. Schematic Representation of (A) Functionalization of CdS QDs with APBA and (B) the Fluorescent Monitoring Procedure of SA Groups on Living Cells

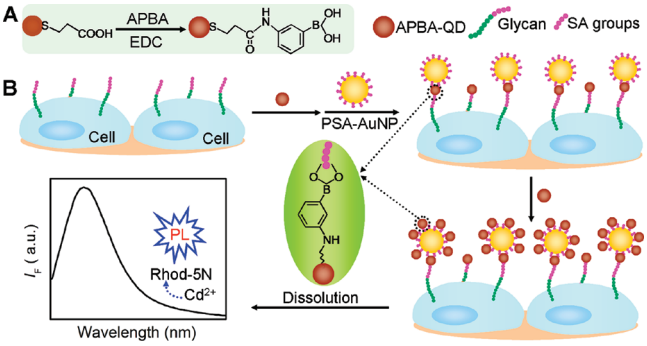

The red color in all confocal images was a pseudocolor, and the emission filter of the confocal microscope was TD 488/543/633. Flow cytometric analysis was performed on FACS Calibar flow cytometer (Becton Dickinson, U.S.A.).

Cell Culture, Treatment, and Viability. The BGC cell line was kindly provided by Affiliated Zhongda Hospital of Southeast University, Nanjing, China. BGC cells were cultured in a flask in RPMI 1640 medium (GIBCO) supplemented with 10% fetal calf serum (FCS, Sigma), penicillin (100 $\mu g\ mL^{-1}$), and streptomycin (100 $\mu g\ mL^{-1}$) at 37 °C in a humidified atmosphere containing 5% CO_2. The cells in the exponential growth were collected and separated from the medium by centrifugation at 1000 rpm for 5 min and then washed thrice with sterile 10 mM pH 7.4 PBS. The sediment was resuspended in 10 mM pH 7.4 PBS to obtain a homogeneous cell suspension. Cell number was determined using a Petroff−Hausser cell counter (U.S.A.). Sialidase-treated BGC cells were obtained by incubating the cells in a culture medium containing 10 $\mu g\ mL^{-1}$ sialidase for 20 h. The viability of BGC cells treated with sialidase for different times was determined by counting live cells under a microscope by trypan blue staining, and the values were expressed as percent of control.

Preparation of APBA-Functionalized CdS QDs and FITC. The water-soluble CdS QDs were prepared using MPA as stabilizing agent according to a method reported previously.[42] The obtained QD solution was subjected to ultrafiltration using a Vivaspin concentrator (Sartorius, 10000 MW) at 10 000*g* for 10 min to remove excessive MPA. The upper phase was washed twice with water and diluted to a certain concentration with pH 7.4 PBS. The resulting CdS QD solution could be stable for 3 months, and its concentration and the size of the QDs were detected with the UV−vis absorption.

An amount of 0.5 mL of MPA-capped CdS QD solution (10 μM) was mixed with the mixture of EDC (3 mg in 50 μL of PBS) and APBA (0.45 mL, 2 mM in PBS) for conjugation of QDs and APBA (Scheme 1A). After incubation for 3 h at 25 °C under shaking and free of light, the resulting sample was ultrafiltrated using a Vivaspin concentrator (Sartorius, 10000 MW) at 10 000*g* for 12 min at 4 °C to remove the nonconjugated APBA. The obtained conjugates were washed thrice with pH 7.4 PBS by ultrafiltration to obtain APBA−QDs (~20 μM), which were kept at 4 °C prior to use. The average number of APBA ligands on each QD was calculated to be 140 according to the previous protocol.[34] Briefly, the concentration of nonconjugated APBA in

the filtrate was acquired by comparing its absorption value at 291 nm to a standard curve, and the obtained result was used to calculate the number of APBA conjugated to QDs.

The APBA-functionalized FITC was synthesized as follows. APBA (41 mg, 0.30 mmol) and FITC (80 mg, 0.21 mmol) were first dissolved in methanol (50 mL). After reaction for 24 h at 30 °C under stirring and free of light, the resulting mixture was concentrated and evaporated under reduced pressure. The residue was then purified by silica gel column chromatography (EtOAc/EtOH 5:1) and evaporated under reduced pressure to afford APBA−FITC (49.6 mg, 62%) as an orange-yellow powder.

Preparation of Glyconanoparticles. The glyconanoparticles were prepared through the direct reduction of $HAuCl_4$ by citrate using PSA as the stabilizing reagent. The solution (50.0 mL) for preparation of PSA−AuNPs contained 0.01% $HAuCl_4$ and 0.068 mg mL^{-1} PSA. After the mixture was heated to 80 °C with a water bath and continuously stirred for 15 min, 1.68 mL of 10 mg mL^{-1} sodium citrate solution was rapidly added to the mixture. The resulting mixture was then allowed to stir for 1 h at 80 °C. Afterward, a clear red glyconanoparticle solution could be obtained. To obviate the nonspecific adsorption of PSA−AuNPs, BSA was used to block the glyconanoparticles by adding 1 mL of a 1% BSA solution to 20 mL of the freshly prepared PSA−AuNPs solution under stirring. After 1 h, the resultant solution was centrifuged at 12 000*g* for 30 min. The precipitate was then thrice washed in PBS by centrifugation to remove the excessive PSA and BSA and resuspended with PBS. The as-prepared solution of PSA−AuNPs (~0.1 μM) was kept at 4 °C.

Cell Surface Carbohydrate Analysis. An amount of 40 μL of BGC cells at different concentrations was seeded in microplate wells and incubated for 4 h under the same conditions as those for cell culture. After the culture solution was removed, the microplate wells were blocked with 1% BSA for 30 min. After the cells were washed thrice with pH 7.4 PBS, the cells were incubated with 50 μL of 1 μM APBA−QD solution (Scheme 1B). After the specific conjugation between APBA−QDs and SA groups on cells for 30 min at 37 °C, the microplate wells were washed thrice with PBS, and 50 μL of 50 nM PSA−AuNPs was added to each well and incubated at 37 °C for 30 min. After the microplates were carefully washed thrice with PBS, 50 μL of 1 μM APBA−QDs solution was added to each well for the third incubation at 37 °C for 30 min. The microplates were then carefully washed thrice with PBS to remove the nontagged APBA−QD probe, and 60 μL of 0.1 M HNO_3 was added to each well to dissolve the tagged QDs.

The HNO_3-treated mixture was diluted to 0.6 mL with PBS and centrifuged at 1000*g* for 5 min to obtain a supernatant. After adjusting the pH of the supernatant to 7.4 using 1 M NaOH, 300 μL of the resulting Cd^{2+} solution containing 3 μM Rhod-5N was detected with a F900 fluorescence spectrometer at room temperature, using the excitation wavelength of 540 nm. The emission spectrum from 550 to 650 nm was collected with a slit width of 2 nm.

Flow Cytometric Analysis of Carbohydrate Expression on BGC Cells. BGC cells in the exponential growth phase were collected and separated from the medium by centrifugation at 1000 rpm at room temperature for 6 min. Subsequently, the cells were washed with sterile cold pH 7.4 PBS and resuspended in the PBS. The cell concentration was determined. An amount of 50 μL of 1×10^7 cells mL^{-1} cell suspension was then added to the mixture of 445 μL of PBS and 5 μL of 2 mg mL^{-1} APBA−FITC. After incubation for 30 min, the cells were collected by centrifugation at 1000 rpm for 6 min, washed twice with 200 μL of cold PBS, resuspended in 500 μL of PBS, and assayed by flow cytometry. Unlabeled BGC cells were used as the negative control for estimation of autofluorescence, and relative cell-associated fluorescent intensity was obtained by subtraction of autofluorescence.

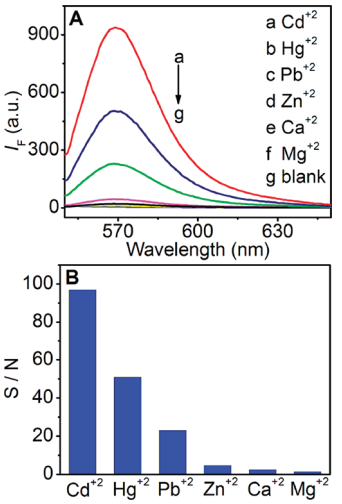

Figure 1. (A) Fluorescence spectra of 3 μM Rhod-5N in the presence of 20 μM metal cations and (B) ratios of fluorescence intensities of the complex of Rhod-5N and metal cations to Rhod-5N at 569 nm.

RESULTS AND DISCUSSION

Design of the Signal Amplification Strategy. As shown in Scheme 1B, APBA−CdS QDs were first coupled to the SA groups on cells at the physiological pH value of 7.4. In order to obtain double signal amplification, following the conjugation of PSA−AuNPs to the APBA−QDs attached on the cell surface, much more APBA−QDs were enriched on the cell surface through the glyconanoparticles, and cadmic cation was released from the captured QDs to trigger the strong fluorescence of the metal-responsive dye Rhod-5N. The fluorescence intensity, recorded at 569 nm with an excitation wavelength of 540 nm, was directly related to the amount of APBA−QDs on the cells and, thus, reflected the expression extent of SA groups on BGC cells and the amount of cells in the microplate well, providing a strategy for monitoring the cell concentration and the SA expression on living cells.

Rhod-5N is a nonfluorescent metal-sensitive dye and has higher affinity to Cd^{2+} than many other metal ions such as Ca^{2+} and Zn^{2+}.[40,41] Thus Cd^{2+} can trigger much stronger fluorescence intensity (I_F) of Rhod-5N than other metal ions with the similar peak wavelength,[41] as shown in Figure 1A. As a nonfluorescent dye in the studied wavelength range, Rhod-5N shows very weak fluorescent signal (Figure 1A, curve g), which could be thought as a noise in the proposed detection. The complex of Rhod-5N and Cd^{2+} showed the highest signal-to-noise ratio at 569 nm (Figure 1B). Thus, the proposed fluorescent detection system could produce high sensitivity with very low background for bioanalysis.

Characterization of APBA−CdS QD Conjugates and PSA−AuNPs. The UV−vis absorption peak of MPA-capped CdS QDs occurred at 427 nm (not shown), from which the size of the QDs and the concentration of QD solution could be estimated to be

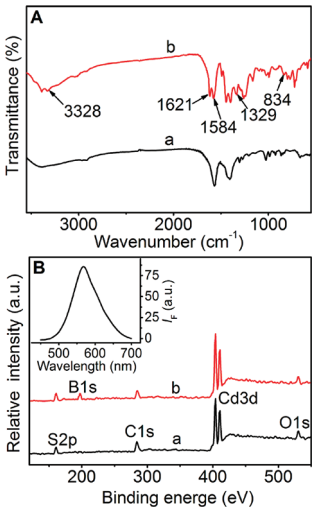

Figure 2. (A) FT-IR and (B) XPS spectra of (a) CdS QDs and (b) APBA-functionalized CdS QDs. Inset in panel B: fluorescence spectrum of APBA−QDs in pH 7.4 PBS.

3.1 nm and 76 μmol L^{-1} based on Peng's empirical equations.[43] For introducing PBA ligand to the QD surface, APBA was used to link the carboxylic group on QDs in the presence of EDC. The fluorescence spectrum of the APBA−QDs solution showed an emission peak at 567 nm (inset in Figure 2B). Using rhodamine B as a standard control, the fluorescence quantum yield of APBA−QDs was calculated to be 8.6%. The obtained APBA−QDs could be confirmed by FT-IR and XPS spectra (Figure 2).

In comparison with the FT-IR spectrum of the CdS QDs (Figure 2A, curve a), the FT-IR spectrum of the resulting APBA−QDs (Figure 2A, curve b) displayed obvious absorption peaks corresponding to the B−O stretching vibration at 1329 cm^{-1} and the C═O and C−N stretching vibrations at 1621 and 1584 cm^{-1}, respectively. In addition, the vibration observed on curve b at 834 and 3328 cm^{-1} could be attributed to the aromatic C−H distortion vibration and amino N−H stretching vibration, respectively. These results indicated that the PBA moieties were successfully immobilized on the QDs. XPS were recorded to further analyze the chemical composition of the CdS QDs and APBA−CdS QDs (Figure 2B). Compared with the XPS spectrum of CdS QDs (Figure 2B, curve a), the spectrum of APBA−CdS QDs (Figure 2B, curve b) showed a new and obvious peak at 197.8 eV, which corresponded to B1s. This result further confirmed the formation of PBA moieties on the QD surfaces.

The red-colored solution of PSA−AuNPs exhibited a UV−vis absorption peak centered at 521 nm (Figure 3A), a typical surface plasmon resonance band for AuNPs, indicating the formation of AuNPs. The TEM photo of the PSA−AuNPs showed a uniform spherical shape and monodispersity with a diameter of 13 nm (Figure 3B). The size of PSA−AuNPs was also analyzed by dynamic light scattering. As shown in the inset in Figure 3A, the average size of PSA−AuNPs was about 13 nm, which was in accordance with the result from the TEM image (Figure 3B). Thus, the value of theoretical stoichiometry of the APBA−QD/PSA−AuNP ratio could be obtained to be 55. The conjugation between PSA and AuNPs resulted from the interaction between AuNPs and the amine groups of PSA.[44] In addition, the interaction of the oxygen-to-gold dative bond could also be formed between the hydroxyl group of PSA and the gold atom.[45] As a result, a high binding affinity could be obtained between PSA and

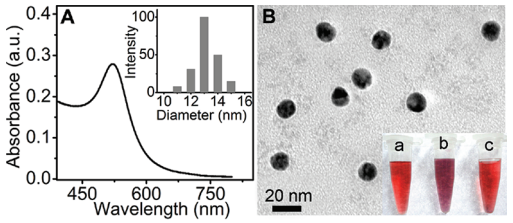

Figure 3. (A) UV−vis spectrum and (B) TEM image of PSA−AuNPs. Inset in panel A: diameter distribution of PSA−AuNPs obtained from dynamic light scattering measurement. Inset in panel B: photos of tubes after mixing 180 μL of 50 nM PSA−AuNPs with 20 μL of (a) PBS, (b) 1 μM APBA−QDs, and (c) 1 μM QDs in 10 mM pH 7.4 PBS for 30 min.

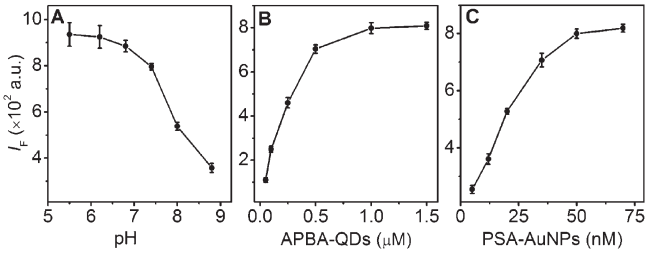

Figure 4. Dependence of I_F for 1 × 10^6 cells mL^{-1} BGC cells on (A) pH for coupling PBA moieties to SA groups, (B) APBA−QDs concentration, and (C) PSA−AuNPs concentration; when one parameter changes the others are under their optimal conditions.

AuNPs, which ensured the stability of the formed glyconanoparticles. After blocking the surface-active sites of glyconanoparticles with BSA for preventing the nonspecific interaction, the obtained glyconanoparticles could be stable in PBS for several months.

The prepared PSA−AuNP solution showed a stable red color, which was the characteristic color of dispersed AuNPs (inset in Figure 3B, photo a). After APBA−QDs were added to the PSA−AuNP solution for 30 min, the solution became purple owing to the red-shifted plasmon band of the PSA−AuNP (inset in Figure 3B, photo b), which was a well-understood feature of the aggregation process,[46] whereas the PSA−AuNPs incubated with QDs solution did not show any distinguishable change (inset in Figure 3B, photo c). The formation of the aggregate was therefore attributed to the cross-linking of PSA−AuNPs by APBA−QDs with PBA moieties. This result demonstrated the successful construction of the PSA−AuNPs and APBA−QDs and their specific interaction.

Condition Optimization for Conjugation of APBA−QDs to Cell Surface. The effect of pH on the binding of PBA moieties to SA groups on BGC cells was investigated in presence of 1 × 10^6 cells mL^{-1} BGC cells at 37 °C. As shown in Figure 4A, the fluorescence signal increased greatly as the pH changed from 8.8 to 6.8, followed with a slight increase in the pH range of 6.8−5.5. This result was in good agreement with the previous reports,[32,33] which suggested that PBA moieties could form favorable binding with SA on the cell surface at the physiological pH of 7.4. Although operation under weak acidic condition could undoubtedly lead to slightly enhanced detection sensitivity, physiological pH condition was chosen to retain the biological activity of living cells for the detection of cell surface SA groups.

The analytical performance of the designed strategy was related to the concentration of APBA−QDs and PSA−AuNPs

dx.doi.org/10.1021/ac201488x |Anal. Chem. 2011, 83, 7006–7012

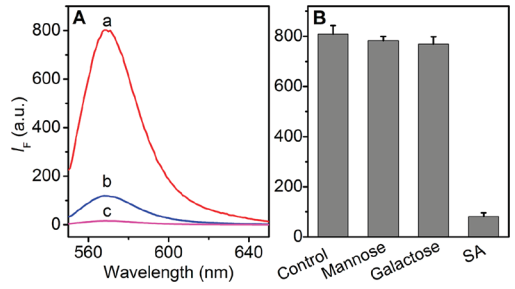

Figure 5. (A) Fluorescence spectra of Rhod-5N triggered by cadmic cation responding to 1 μM APBA−QDs treated 1.0 × 10^6 cells mL^{-1} BGC cells (a) with and (b) without PSA−AuNPs for signal amplification and (c) 1 μM APBA−QDs treated microplate well in the absence of cells as control, and (B) monosaccharide inhibition assay by preincubating APBA−QDs in 1 mM mannose, galactose, or SA for 30 min before incubation with 1.0 × 10^6 cells mL^{-1} BGC cells in 10 mM, pH 7.4 PBS.

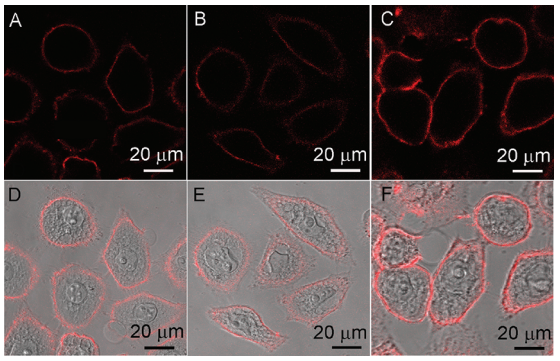

Figure 6. Confocal fluorescence (A−C) and overlapped fluorescence and bright-field images (D−F) of BGC cells after being treated with APBA−QDs (A and D), APBA−QDs and then PSA−AuNPs (B and E), and APBA−QDs, PSA−AuNPs, and APBA−QDs (C and F) under the optimal experiment conditions.

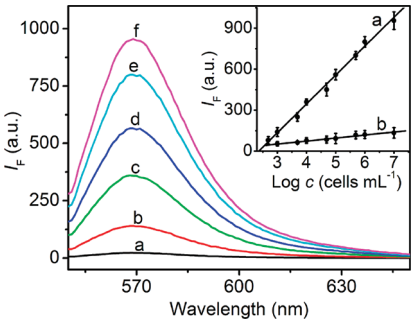

Figure 7. Fluorescence spectra of Rhod-5N triggered by cadmic cation responding to 0, 1.0 × 10^3, 1.0 × 10^4, 1.0 × 10^5, 1.0 × 10^6, and 1.0 × 10^7 cells mL^{-1} BGC cells (from a to f). Inset: plots of I_F vs logarithm of cell concentration (a) with and (b) without PSA−AuNPs for signal amplification.

used in the incubation solution for forming saturated binding of the recognition sites. In 10 mM pH 7.4 PBS the cadmium cation triggered fluorescence signal of 3 μM Rhod-5N increased with the increasing concentrations of APBA−QDs and PSA−AuNPs from 0.05 to 0.5 μM and 5 to 35 nM, respectively, and then maintained the maximum value at higher concentrations (Figure 4, parts B and C). Therefore, the optimal concentrations of APBA−QDs and PSA−AuNPs were selected at 1 μM and 50 nM, respectively.

Performance and Specificity of Signal Amplification. After the attached QDs were dissolved from the cell surface, the fluorescence of Rhod-5N triggered by the dissolved cadmic cation reporter could be conveniently detected. The PSA−AuNPs amplification produced 7 times stronger fluorescence signal at 1 × 10^6 cells mL^{-1} BGC cells (Figure 5A, curves a and b), whereas the resulting solution in the absence of the cells showed neglectable fluorescence response, indicative of very little nonspecific adsorption of APBA−QDs and SA−AuNPs on the wall of the microplate wells (Figure 5A, curve c). Thus, the signal amplification strategy could greatly enhance the fluorescent intensity and did not visibly increase the background response, leading to highly sensitive detection.

To validate the recognition specificity of PBA moieties to cell surface SA groups, monosaccharide inhibition assay was carried out by replacing APBA−QDs with inhibited APBA−QDs which were preincubated with 1 mM mannose, galactose, or SA for 30 min before incubation with 1.0 × 10^6 cells mL^{-1} BGC cells. As shown in Figure 5B, SA notably inhibited the binding of PBA moieties to cell surface SA groups, whereas mannose and galactose did not show any obvious inhibition in 10 mM pH 7.4 PBS. This result was in accord with previous reports[32,33] and suggested that the APBA−QDs could allow highly specific and efficient binding of SA groups on living cells.

The confocal images of BGC cells during the detection procedure were used to validate the designed signal amplification method. As shown in Figure 6, the weak fluorescence of QDs was observed after APBA−QDs were coupled to the SA groups on cells. Following the conjugation of PSA−AuNPs to the attached APBA−QDs through the APBA−SA recognition, the fluorescent signal did not show remarkable decrease, indicating little binding competition of APBA−QDs between cells and PSA−AuNPs. This result was attributed to the multiplex binding of APBA−QDs to both glycan groups on the cell surface and PSA−AuNPs. After the further enrichment of APBA−QDs to the attached PSA−AuNPs, the confocal image showed enhanced fluorescence of QDs with a uniform and obvious ring-shaped profile, which excluded the endocytosis of APBA−QDs by living cells and illuminated the signal amplification process. The thickness of PSA coating on PSA−AuNPs was calculated to be 5 nm by comparing the sizes of AuNPs in presence and absence of PSA in the DLS measurement. The thick PSA coating and the low fluorescence quantum yield of QDs could minimize the fluorescence quenching of APBA−QDs caused by PSA−AuNPs.[47]

Cell Detection. In view of the outstanding ability for signal amplification, the dynamic range of the designed method for detection of BGC cells was examined. Under the optimal conditions, the I_F was proportional to the logarithmic value of the cell concentration ranging from 5.0 × 10^2 to 1.0 × 10^7 cells mL^{-1} with a correlation coefficient R of 0.996 (n = 9) (Figure 7). The limit of detection for cell concentration was calculated to be 210 cells mL^{-1} at 3σ, which was comparable with those of 620 cells mL^{-1} at an electrochemical cytosensor for detection of BGC cells[24] and 750 cells mL^{-1} at a quartz crystal microbalance biosensor for detection of *Escherichia coli*[48] and much lower than that of 6000 cells mL^{-1} at an immunosensor chip for detection of *E. coli* O157:H7[49] and 1.0 × 10^4 cells mL^{-1} at an immunosensor for detection of *Salmonella* species based on a quartz crystal microbalance.[50] Considering the fact that the volume of BGC cell suspension for incubation step was only 40 μL, the designed

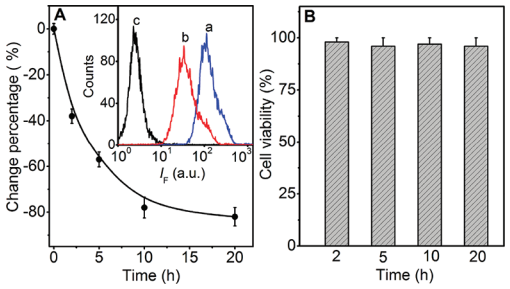

Figure 8. (A) Time-dependent effect of sialidase on SA expression on BGC cells and (B) viability of BGC cells treated with sialidase for different times. The change percentage (Δ%) was calculated as follows: $\Delta\% = [T/C - 1] \times 100\%$, where T and C are the I_F obtained on sialidase-treated or control BGC cells. Inset in panel A: flow cytometric analysis of SA groups expressed on BGC cells (a) before and (b) after sialidase treatment for 20 h with APBA-functionalized FITC, and (c) autofluorescence of unlabeled BGC cells.

strategy achieved the limit of eight BGC cells. The low detection limit was attributed to the double signal amplification.

In order to demonstrate the enhanced sensitivity of the proposed strategy, an APBA−QD-based method without PSA−AuNPs for further enrichment was designed as a control. Under the same optimal conditions, the change of I_F was slight upon the increasing cell concentration (inset in Figure 7, curve b). PSA−AuNPs amplification led to a 10 times higher slope than single-step binding of APBA−QDs to cell surface SA, verifying the greatly improved sensitivity.

At the cell concentrations of 1.0×10^4 and 1.0×10^6 cells mL^{-1}, the proposed method showed the relative standard deviations of 6.1% and 4.7% examined for five determinations, respectively, showing good reproducibility. The 10-fold higher slope and the good reproducibility indicated that the sensitivity and the accuracy of the results were not affected by the difference in affinity for APBA to the cell surface and PSA. Thus, the designed strategy showed good performance for detection of cancer cells with broad detection range, low detection limit, good reproducibility, and a simple detection procedure.

Dynamic Monitoring of Cell Surface Carbohydrate Expression. The high sensitivity and facility of the proposed strategy allowed it to be further used in monitoring of the dynamic alteration of carbohydrate expression on living cells in response to sialidase. Sialidase is usually utilized as a cleaving agent for all forms of SA components present in glycoconjugates,[51] and its activity can regulate cell surface glycan expression.[52,53] At the same amount of sialidase-treated cells used for the detection process, the difference of fluorescent signal could be attributed to the varying expression level of SA on cell surface upon sialidase treatment. The assessment of cell surface SA expression was implemented by comparing the different expression extent of SA on sialidase-treated cells over time with the control cells of 1.0×10^6 cells mL^{-1} using the designed strategy. During treatment with sialidase over 20 h, the sialidase-treated cells revealed a progressively decreased change of response compared to untreated cells as a control (Figure 8A). This result indicated the decrease of terminal SA on sialidase-treated BGC cells. After being treated for 20 h the SA groups on sialidase-treated BGC cells decreased by 82%. The viability of BGC cells after being treated with sialidase for different times was verified by comparing to control cells (Figure 8B). After treatment with sialidase for 20 h, the cells exhibited 96.2% viability, indicating favorable cell viability. Before and after sialidase treatment the flow cytometric analysis using APBA-conjugated FITC for SA recognition (inset in Figure 8A) gave the mean fluorescent intensities of 325.7 and 48.3, respectively, showing the change of 85%. This value was compatible with that of 82% obtained from the designed strategy, suggesting acceptable reliability of the proposed method for evaluation of cell surface carbohydrates.

CONCLUSIONS

A versatile method has been developed for highly sensitive and selective in situ evaluation of cell surface SA groups by combining the multiplex sandwich binding of the APBA−QD probes to SA groups on living cells and glyconanoparticles and the sensitive fluorescence detection of metal-responsive dye. This method utilizes a novel chemical molecular borate ligand for SA binding and contains double signal amplification: the specific enrichment of APBA−QDs on glyconanoparticles and cadmium cation triggered fluorescence emission of the dye. It possesses high specificity and acceptable reproducibility. The double signal amplification strategy can be used for both highly sensitive detection of cell concentration with a wide dynamic range and monitoring of dynamic change in cell surface carbohydrate expression in response to enzyme and could be expanded with the addition of PBA derivatives to other glycans to the repertoire. It could be anticipated that this proposed strategy would provide a significant analytical tool to meet the challenges in elucidation of the complex mechanisms underlying carbohydrate-related biological processes.

AUTHOR INFORMATION

Corresponding Author

*Phone and Fax: +86-25-83593593. E-mail: hxju@nju.edu.cn.

ACKNOWLEDGMENT

We gratefully acknowledge the National Basic Research Program of China (2010CB732400), National Natural Science Foundation of China (20821063, 21005037, 20875044), Ph.D. Fund for Young Teachers (20100091120034), and Natural Science Foundation of Jiangsu (BK2010193, BK2008014).

REFERENCES

(1) Spiro, R. G. *Glycobiology* **2002**, *12*, 43R–56R.
(2) Tian, Y.; Zhou, Y.; Elliott, S.; Aebersold, R.; Zhang, H. *Nat. Protoc.* **2007**, *2*, 334–339.
(3) Dube, D. H.; Bertozzi, C. R. *Nat. Rev. Drug Discovery* **2005**, *4*, 477–488.
(4) Varki, A. *Glycobiology* **1993**, *3*, 97–130.
(5) Ohtsubo, K.; Marth, J. D. *Cell* **2006**, *126*, 855–867.
(6) Marth, J. D.; Grewal, P. K. *Nat. Rev. Immunol.* **2008**, *8*, 874–887.
(7) Chen, I. J.; Chen, H. L.; Demetriou, M. *J. Biol. Chem.* **2007**, *282*, 35361–35372.
(8) Crocker, P. R.; Feizi, T. *Curr. Opin. Struct. Biol.* **1996**, *6*, 679–691.
(9) Feizi, T. *Immunol. Rev.* **2000**, *173*, 79–88.
(10) Bertozzi, C. R.; Kiessling, L. L. *Science* **2001**, *291*, 2357–2364.
(11) Qiu, Y.; Patwa, T. H.; Xu, L.; Shedden, K.; Misek, D. E.; Tuck, M.; Jin, G.; Ruffin, M. T.; Turgeon, D. K.; Synal, S.; Bresalier, R.; Marcon, N.; Brenner, D. E.; Lubman, D. M. *J. Proteome Res.* **2008**, *7*, 1693–1703.
(12) Lin, S.; Kemmner, W.; Grigull, S.; Schlag, P. M. *Exp. Cell Res.* **2002**, *276*, 101–110.
(13) Hakomori, S. *Cancer Res.* **1996**, *56*, 5309–5318.

(14) Krishnamoorthy, L.; Mahal, L. K. *ACS Chem. Biol.* **2009**, *4*, 715–732.
(15) Szymanski, C. M.; Michael, F. S.; Jarrell, H. C.; Li, J. J.; Gilbert, M.; Larocque, S.; Vinogradov, E.; Brisson, J. R. *J. Biol. Chem.* **2003**, *278*, 24509–24520.
(16) Kaji, H.; Saito, H.; Yamauchi, Y.; Shinkawa, T.; Taoka, M.; Hirabayashi, J.; Kasai, K.; Takahashi, N.; Isobe, T. *Nat. Biotechnol.* **2003**, *21*, 667–672.
(17) Lis, H.; Sharon, N. *Chem. Rev.* **1998**, *98*, 637–674.
(18) Agard, N. J.; Bertozzi, C. R. *Acc. Chem. Res.* **2009**, *42*, 788–797.
(19) Hsu, K.; Pilobello, K. T.; Mahal, L. K. *Nat. Chem. Biol.* **2006**, *2*, 153–157.
(20) Pilobello, K. T.; Slawek, D. E.; Mahal, L. K. *Proc. Natl. Acad. Sci. U.S.A.* **2007**, *104*, 11534–11539.
(21) Zheng, T.; Peelen, D.; Smith, L. M. *J. Am. Chem. Soc.* **2005**, *127*, 9982–9983.
(22) Ding, L.; Cheng, W.; Wang, X. J.; Ding, S. J.; Ju, H. X. *J. Am. Chem. Soc.* **2008**, *130*, 7224–7225.
(23) Cheng, W.; Ding, L.; Ding, S. J.; Yin, Y. B.; Ju, H. X. *Angew. Chem., Int. Ed.* **2009**, *48*, 6465–6468.
(24) Cheng, W.; Ding, L.; Lei, J. P.; Ding, S. J.; Ju, H. X. *Anal. Chem.* **2008**, *80*, 3867–3872.
(25) Ding, L.; Ji, Q. J.; Qian, R. C.; Cheng, W.; Ju, H. X. *Anal. Chem.* **2010**, *82*, 1292–1298.
(26) Kohler, J. J. *ChemBioChem* **2009**, *10*, 2147–2150.
(27) Xu, H.; Mao, X.; Zeng, Q.; Wang, S.; Kawde, A.-N.; Liu, G. *Anal. Chem.* **2009**, *81*, 669–675.
(28) Aronoff, S.; Chen, T.; Cheveldayoff, M. *Carbohydr. Res.* **1975**, *40*, 299–309.
(29) Lorand, J. P.; Edwards, J. O. *J. Org. Chem.* **1959**, *24*, 769–774.
(30) Dowlut, M.; Hall, D. G. *J. Am. Chem. Soc.* **2006**, *128*, 4226–4227.
(31) Otsuka, H.; Uchimura, E.; Koshino, H.; Okano, T.; Kataoka, K. *J. Am. Chem. Soc.* **2003**, *125*, 3493–3502.
(32) Matsumoto, A.; Sato, N.; Kataoka, K.; Miyahara, Y. *J. Am. Chem. Soc.* **2009**, *131*, 12022–12023.
(33) Matsumoto, A.; Cabral, H.; Sato, N.; Kataoka, K.; Miyahara, Y. *Angew. Chem., Int. Ed.* **2010**, *49*, 5494–5497.
(34) Liu, A. P.; Peng, S.; Soo, J. C.; Kuang, M.; Cheng, P.; Duan, H. W. *Anal. Chem.* **2011**, *83*, 1124–1130.
(35) Nam, J. M.; Thaxton, C. S.; Mirkin, C. A. *Science* **2003**, *301*, 1884–1886.
(36) Rosi, N. L.; Mirkin, C. A. *Chem. Rev.* **2005**, *105*, 1547–1562.
(37) Liu, G. D.; Wang, J.; Kim, J.; Jan, M. R. *Anal. Chem.* **2004**, *76*, 7126–7130.
(38) Gill, R.; Zayats, M.; Willner, I. *Angew. Chem., Int. Ed.* **2008**, *47*, 7602–7625.
(39) Wang, J.; Liu, G.; Merkocüi, A. *J. Am. Chem. Soc.* **2003**, *125*, 3214–3215.
(40) Li, J. S.; Zhang, T. R.; Ge, J. P.; Yin, Y. D; Zhong, W. W. *Angew. Chem., Int. Ed.* **2009**, *48*, 1588–1591.
(41) Li, J. S.; Schachermeyer, S.; Wang, Y.; Yin, Y. D.; Zhong, W. W. *Anal. Chem.* **2009**, *81*, 9723–9729.
(42) Han, E.; Ding, L.; Jin, S.; Ju, H. X. *Biosens. Bioelectron.* **2011**, *26*, 2500–2505.
(43) Yu, W. W.; Qu, L. H.; Guo, W. Z.; Peng, X. G. *Chem. Mater.* **2003**, *15*, 2854–2860.
(44) Cui, R. J.; Pan, H. C.; Zhu, J. J.; Chen, H. Y. *Anal. Chem.* **2007**, *79*, 8494–8501.
(45) Calzolari, A.; Cicero, G.; Cavazzoni, C.; Felice, R. D.; Catellani, A.; Corni, S. *J. Am. Chem. Soc.* **2010**, *132*, 4790–4795.
(46) Elghanian, R.; Storhoff, J. J.; Mucic, R. C.; Letsinger, R. L.; Mirkin, C. A. *Science* **1997**, *277*, 1078–1081.
(47) Dezhurov, S. V.; Volkova, I. Y.; Wakstein, M. S. *Bioconjugate Chem.* **2011**, *22*, 338–345.
(48) Shen, Z. H.; Huang, M. C.; Xiao, C. D.; Zhang, Y.; Zeng, X. Q.; Wang, P. G. *Anal. Chem.* **2007**, *79*, 2312–2319.
(49) Ruan, C. M.; Yang, L. J.; Li, Y. B. *Anal. Chem.* **2002**, *74*, 4814–4820.
(50) Wong, Y. Y.; Ng, S. P.; Ng, M. H.; Si, S. H.; Yao, S. Z.; Fung, Y. S. *Biosens. Bioelectron.* **2002**, *17*, 676–684.
(51) Fukuda, M.; Bao, X. F. *Nat. Chem. Biol.* **2008**, *4*, 721–722.
(52) Gadhoum, S. Z.; Sackstein, R. *Nat. Chem. Biol.* **2008**, *4*, 751–757.
(53) Parker, R. B.; Kohler, J. J. *ACS Chem. Biol.* **2010**, *5*, 35–46.